Crystal Growth, Structure, and Magnetic Properties of a New Polymorph of $Fe_2P_2O_7$

Carmen Parada,[†] Josefina Perles,[‡] Regino Sáez-Puche,[†] Caridad Ruiz-Valero,*[,‡] and Natalia Snejko[‡]

Instituto de Ciencia de Materiales de Madrid, CSIC, Cantoblanco, E-28049 Madrid, Spain, and Departamento de Química Inorgánica, Facultad de Ciencias Químicas, Universidad Complutense de Madrid, E-28040 Madrid, Spain

Received March 10, 2003. Revised Manuscript Received June 4, 2003

The title compound, a new polymorphic phase of iron diphosphate, was prepared by solid-state reaction. This compound crystallizes in the monoclinic space group $P2_1/c$ with $a = 4.4668(6)$ Å, $b = 9.896(1)$ Å, $c = 5.2077(7)$ Å, $\beta = 97.516(2)°$, $V = 228.22(5)$ Å^3, and $Z = 2$. The structure is characterized by the arrangement of FeO_6 octahedra and P_2O_7 groups. The FeO_6 octahedra are connected by edge sharing to form six-membered rings, which are further interconnected to form two-dimensional zigzag sheets perpendicular to the [100] direction. The P_2O_7 groups link these sheets to build three-dimensional networks. The relation between $Fe_2P_2O_7$ polymorphs is discussed. Magnetic measurements reveal the presence of antiferromagnetic interactions in the Fe^{2+} sublattice at about 12.5 K. Magnetization isotherms obtained below the Neel temperature follow a linear variation in the whole range of the magnetic field strength characteristic of the mentioned antiferromagnetic order and metamagnetic (field induced) transitions have not been observed up to 5 T.

1. Introduction

Following our work on phosphates[1−6] of transition metal cations, we are interested in the Fe−O−P system that presents numerous compounds, and many of them exist as minerals, for instance, the vivianite, the triphylite, or the rockbridgite. Many of these compounds have been subjected to intense research for the past few years, mainly for their interesting crystal chemistry and more recently for their attractive properties.[7−9] $Fe_2P_2O_7$ was obtained for the first time by Royen and Korinth,[10] and they reported the synthesis and the powder diagram. The first structural studies using single crystals were realized by Stefanidis and Nord[11] assuming the non-centrosymmetric $P1$ space group. Later, Hoggins et al.[12] described the same compound with the nonconventional $C\bar{1}$ space group to compare the unit cell with that of the other monoclinic $M_2P_2O_7$ (M = Mn, Cu, Mg, Zn). The conclusion was that this diphosphate, with thortveitite structure, is isostructural with the β polymorph (or high-temperature form) of $Mg_2P_2O_7$. In fact, it is a triclinic distortion of this form. It has to be noticed that the divalent metal diphosphates $M_2P_2O_7$ are, in general, polymorphic, and in this paper, we present the synthesis, crystal structure determination, and magnetic properties of the new higher temperature form (denoted as γ hereafter) of $Fe_2P_2O_7$.

2. Experimental Section

Synthesis. Single crystals of γ-$Fe_2P_2O_7$ were grown by melting a mixture of analytical-grade iron(II) oxalate dihydrate and ammonium dihydrogen phosphate, in a molar ratio of 1:1. After grinding, the mixture was heated in a closed porcelain crucible to a final temperature of 700 °C with intermediate grindings at 250 and 350 °C, to make the mixture homogeneous. The furnace was kept at these temperatures for 3 h and then the molten solid formed was slowly cooled to 200 °C at a rate of 10 °C/h, and from this value to room temperature at 50 °C/h. At the end of this process, many prismatic single crystals, yellow-orange in color, were obtained on the surface of the cake melt. These crystals were mechanically separated from the remaining compact yellow powder using an appropriate sieve and were suitable for solving the crystal structure and to measure the magnetic properties.

Structure Determination. Single-Crystal X-ray Diffraction. A summary of the conditions for data collection is given in Table 1. A yellow-orange crystal of prismatic shape was resin epoxy-coated and mounted on a Siemens Smart CCD

* To whom correspondence should be addressed. Telephone: +34 91 334 90 26. Fax: +34 91 372 0623. E-mail: crvalero@icmm.csic.es.
† Universidad Complutense de Madrid.
‡ Instituto de Ciencia de Materiales de Madrid, CSIC.

(1) Sanz, F.; Parada, C.; Amador, U.; Monge, M. A.; Ruiz-Valero, C. *J. Solid State Chem.* **1996**, *123*, 129.
(2) Sanz, F.; Parada, C.; Rojo, J. M.; Ruiz-Valero, C.; Saez-Puche, R. *J. Solid State Chem.* **1999**, *145*, 604.
(3) Sanz, F.; Parada, C.; Rojo, J. M.; Ruiz-Valero, C. *Chem. Mater.* **1999**, *11*, 2673.
(4) Sanz, F.; Parada, C.; Ruiz-Valero, C. *Chem. Mater.* **2000**, *12*, 671.
(5) Sanz, F.; Parada, C.; Rojo, J. M.; Ruiz-Valero, C. *Chem. Mater.* **2001**, *13*, 1334.
(6) Sanz, F.; Parada, C.; Ruiz-Valero, C. *J. Mater. Chem.* **2001**, *11*, 208.
(7) Durif, A. *Crystal Chemistry of Condensed Phosphates*; Plenum Press: New York, 1995.
(8) Padhi, A. K.; Nanjundaswamy, K. S.; Masquelier, C.; Goodenough, J. B. *J. Electrochem. Soc.* **1997**, *144*, 2581.
(9) Wurm, C.; Morcrette, M.; Rousse, G.; Dupont, L.; Masquelier, C. *Chem. Mater.* **2002**, *14*, 2701.
(10) Royen, P.; Korinth, J. *Z. Anorg. Allg. Chem.* **1957**, *291*, 227.
(11) Stefanidis, T.; Nord, A. G. *Z. Kristallogr.* **1982**, *159*, 255.
(12) Hoggins, J. T.; Swinnea, J. S.; Steinfink, H. *J. Solid State Chem.* **1983**, *47*, 278.

10.1021/cm034137a CCC: $25.00 © 2003 American Chemical Society
Published on Web 07/24/2003

Table 1. Crystal Data and Structure Refinement for γ-$Fe_2P_2O_7$

formula	$Fe_2P_2O_7$
temperature (K)	296
molar weight (g/mol)	285.64
crystal system	monoclinic
space group	$P2_1/c$
a (Å)	4.4668(6)
b (Å)	9.896(1)
c (Å)	5.2077(7)
β (°)	97.516(2)
cell volume (Å^3)	228.22(5)
Z	2
calc. density (g/cm^3)	4.157
F(000)	276
μ (mm^{-1})	7.035
dimensions (mm)	0.20 × 0.25 × 0.30
radiation	Mo Kα (0.71073 Å)
diffractometer	Bruker-SMART-CCD
limiting indices	(−6, −10, −7) to (5, 14, 6)
θ range for data collected	4.12−31.3
reflections collected	1711
independent reflections	684
data/restraints/parameters	684/0/52
goodness-of-fit on F^2	1.055
final R indices [$I > 2\sigma(I)$]	$R_1 = 0.0414$, $R_2 = 0.1070$
R indices (all data)	$R_1 = 0.0495$, $R_2 = 0.1103$

diffractometer equipped with a normal focus, 2.4-kW sealed tube X-ray source (Mo Kα radiation, $\lambda = 0.71073$ Å) operating at 40 kV and 20 mA. Data were collected over a hemisphere of reciprocal space by a combination of three sets of exposures. Each set had a different φ angle for the crystal and each exposure of 20 s covered 0.3° in ω. The crystal-to-detector distance was 6.01 cm. Coverage of the unique set was over 99% complete to at least 23° in θ. Unit cell dimensions were determined by a least-squares fit of 40 reflections with $I > 20\sigma(I)$ and $4° < 2\theta < 46°$. The first 30 frames of data were recollected at the end of the data collection to monitor crystal decay. The intensities were corrected for Lorentz and polarization effects. Scattering factors for neutral atoms and anomalous dispersion corrections for Fe and P were taken from the *International Tables for Crystallography*.[13] The structure was solved by Patterson methods and refined in the monoclinic space group $P2_1/c$. Full-matrix least-squares refinement with anisotropic thermal parameters for Fe, P, and O atoms was carried out by minimizing $w(F_o^2 - F_c^2)^2$. Refinement on F^2 for all reflections, weighted R factors (R_w), and all goodness of fit S are based on F^2, while conventional R factors are based on F, R factors based on F^2 are statistically about twice as large as those based on F, and R factors based on all data will be even larger.

All calculations were performed using SMART software for data collection, SAINT[14] for data reduction, SHELXTL[15] to resolve and refine the structure and to prepare material for publication, and ATOMS[16] for molecular graphics.

X-ray Powder Diffraction. The X-ray powder diffraction pattern was taken at room temperature by using a Siemens D-500 diffractometer in the step scan mode, Cu Kα (λ = 1.540598 Å) radiation, at a step value of 0.02°, measuring for 20 s at each step. The observed reflections were indexed on a monoclinic unit cell using the TREOR program[17] in very good agreement with the parameters obtained from the single-crystal X-ray study.

(13) *International Tables for Crystallography*; Kynoch Press: Birmingham, U.K., 1974; Vol. 4, p 72.

(14) Siemens. *SAINT data collection and procedure software for the SMART system*; Siemens Analytical X-ray Instruments, Inc.; Madison, WI, 1995.

(15) Siemens. *SHELXTL*^{TL}, version 5.0; Siemens Analytical X-ray Instruments, Inc.: Madison, WI, 1995.

(16) Dowty, E. *ATOMS for Windows 3.1, a computer program for displaying atomic structures*; Kingsport, TN, 1995.

(17) Smolin, Yu. I.; Shepelev, Yu. F. *Acta Crystallogr.* **1970**, *B26*, 484.

Table 2. Atomic Coordinates and Equivalent Isotropic Displacement Parameters (Å^2 × 10^4), with e.s.d.'s in Parentheses, for γ-$Fe_2P_2O_7$

	multiplicity Wickoff letter	x	y	z	U(eq)[a]
Fe(1)	4e	0.9030(1)	0.1566(1)	0.0841(1)	52(2)
P(1)	4e	0.3584(3)	0.1111(1)	0.6570(2)	78(3)
O(1)	4e	0.6184(8)	0.2036(4)	0.7621(6)	114(7)
O(2)	4e	0.7871(8)	−0.0411(3)	0.1281(6)	132(7)
O(3)	4e	0.1195(7)	0.3206(3)	0.9629(6)	104(6)
O(4)	2d	0.50	0.00	0.50	212(11)

[a] $U(\text{eq}) = {}^1/_3\sum_i\sum_j U_{ij}a_i^*a_j^*a_ia_j$.

Table 3. Selected Bond Distances (Å) and Angles (deg) for γ-$Fe_2P_2O_7$

Fe(1)−O(1)	2.021(3)	Fe(1)−O(1^{i})	2.168(3)
Fe(1)−O(2)	2.044(3)	P(1)−O(1)	1.523(4)
Fe(1)−O(3)	2.032(3)	P(1)−O(2^{iii})	1.532(4)
Fe(1)−O(3^{i})	2.092(3)	P(1)−O(3^{iv})	1.528(3)
Fe(1)−O(2^{ii})	2.201(4)	P(1)−O(4)	1.553(1)
O(1)−Fe(1)−O(2)	99.9(1)	O(3)−Fe(1)−O(2^{ii})	84.4(1)
O(1)−Fe(1)−O(3)	80.3(1)	O(3)−Fe(1)−O(3^{i})	91.6(1)
O(1)−Fe(1)−O(1^{i})	82.4(1)	O(2^{ii})−Fe(1)−O(1^{i})	171.5(1)
O(1)−Fe(1)−O(2^{ii})	94.1(1)	O(2^{ii})−Fe(1)−O(3^{i})	106.6(1)
O(1)−Fe(1)−O(3^{i})	157.0(1)	O(1)−P(1)−O(2^{iii})	112.7(2)
O(2)−Fe(1)−O(3)	159.6(2)	O(1)−P(1)−O(3^{iv})	113.9(2)
O(2)−Fe(1)−O(1^{i})	113.1(1)	O(1)−P(1)−O(4)	105.7(2)
O(2)−Fe(1)−O(2^{ii})	75.2(2)	O(2^{iii})−P(1)−O(3^{iv})	110.9(2)
O(2)−Fe(1)−O(3^{i})	95.2(1)	O(2^{iii})−P(1)−O(4)	107.8(2)
O(3)−Fe(1)−O(1^{i})	87.3(1)	O(3^{iv})−P(1)−O(4)	105.2(1)

[a] Symmetry code: (i) $x, -y + {}^1/_2, z + {}^1/_2$; (ii) $-x, -y, -z + 2$; (iii) $-x - 1, -y, -z + 2$; (iv) $x - 1, -y + {}^1/_2, z - {}^1/_2$.

Magnetic Measurements. The magnetic susceptibility of a polycrystalline sample was measured over the range 2−300 K using a Quantum Design magnetometer and a magnetic field strength of 1000 Oe. Magnetization measurements were made up to 5 T at different temperatures. The experimental susceptibility values were corrected against the diamagnetic contribution of Fe^{2+} and $P_2O_7^{4-}$ ions.

3. Results and Discussion

Crystal Structure. A summary of the fundamental crystal data for γ-$Fe_2P_2O_7$ is given in Table 1. Final atomic coordinates and selected bond distances are given in Tables 2 and 3, respectively.

The structure of γ-$Fe_2P_2O_7$ is characterized by the arrangement of FeO_6 octahedra and P_2O_7 diphosphate groups. This compound is isotypic with the high-temperature form[17] of $Er_2Si_2O_7$, and the most interesting feature of its structure is the existence of P_2O_7 groups with a linear P−O−P bond. The central oxygen atom of the P_2O_7 group is located on the inversion center at ${}^1/_2$, 0, ${}^1/_2$. The iron atom has 6-fold oxygen coordination, forming a distorted octahedron with Fe−O distances ranging from 2.021(3) to 2.201(4) Å. Each FeO_6 octahedron shares three of its edges with its three adjacent Fe neighbors in a hexagonal arrangement (Figure 1), building corrugated layers perpendicular to the [100] direction (Figure 2). Inside a layer, the octahedra arrangement forms large elongated hexagonal voids. The P_2O_7 groups are located above and under these voids, joining the layers to form a three-dimensional structure. Each one of the six peripheral oxygens of the P_2O_7 group is shared with a different FeO_6 octahedron, half of them from the layer above and half of them from the layer underneath. If we compare the β and γ phases, in both of them, the iron atoms lie on

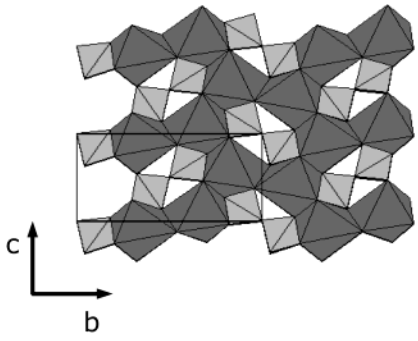

Figure 1. View of the $Fe_2P_2O_7$ structure along [100], showing the six-membered rings formed by FeO_6 octahedra.

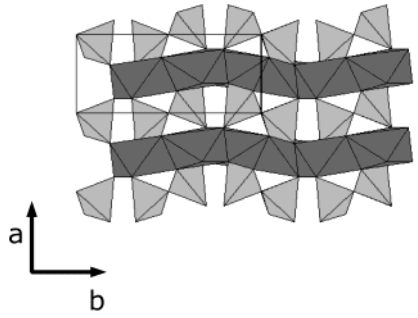

Figure 2. View of the $Fe_2P_2O_7$ structure along [001], showing the P_2O_7 groups linking the $[Fe_6O_{12}]_\infty$ layers.

planes in a two-dimensional hexagonal array (Figure 3). In the β-polymorph, the iron hexagons are placed with their axes parallel to each other, while in the γ-polymorph the axes of two adjacent hexagons in the *b* direction are rotated 90°. This feature can also be observed in the arrangement of the P_2O_7 groups. The Fe−Fe distance is 3.193 Å, slightly shorter than the one in the β-polymorph, 3.236 Å, and the FeO_6 octahedron in the title compound is less distorted, showing better angles and smaller axial distortion (average distances of $Fe-O_{eq}$ 2.047(3) and 2.091(4) Å and of $Fe-O_{ax}$ 2.184-(3) and 2.356(5) Å for the γ and β forms, respectively). The pyrophosphate groups lie along planes between metallic layers and the three geometrical features of P_2O_7 groups are common to the two polymorphs, the distance P−P is 3.10 Å, the P−O−P angle is 180°, and the internal symmetry is an inversion center in both cases.

The bibliographical revision carried out has allowed us to elaborate the classification of diphosphates of formula $M_2P_2O_7$ (where M = first series transition metal), which is shown in Table 4. In our work, we have studied the new higher temperature γ-$Fe_2P_2O_7$ polymorph, and among these γ polymorphs, the Fe, Co, and Ni compounds are isostructural, displaying the Zn compound, a structure completely different from the rest. The high-temperature (β) phases, showing thortveitite structure, are well-known for Mn, Fe, Co, Ni, Cu, and Zn. Each of these pyrophosphates, except for Mn and Fe, which are unknown until the moment in the low-temperature form, display a reversible phase transformation and in each case the room-temperature form is the α phase. The unit cell volume of the α phase is roughly double (in $Cu_2P_2O_7$), quadruple (in $Co_2P_2O_7$ and $Ni_2P_2O_7$), and sextuple (in $Zn_2P_2O_7$) than the corresponding salts of the conjugate β phase. Further, in each case, one axis is always roughly double with a glide plane replacing the mirror plane of the β phase, while another axis remains always unchanged. The third axis, depending on the compound, is equal, double, or triple in the respective α phases. The low-temperature (α) polymorphs of Co and Ni compounds are isostructural, and the analogue of Fe has not been yet described, the reason it is foreseeable that also this low-temperature (α) polymorph could be obtained. The α-$Zn_2P_2O_7$ compound presents a structure different from the rest, as happens also in the γ polymorph.

Magnetic Properties. The reciprocal susceptibility data, $1/\chi$ as a function of the temperature, is shown in Figure 4, inset, also depicted the temperature variation

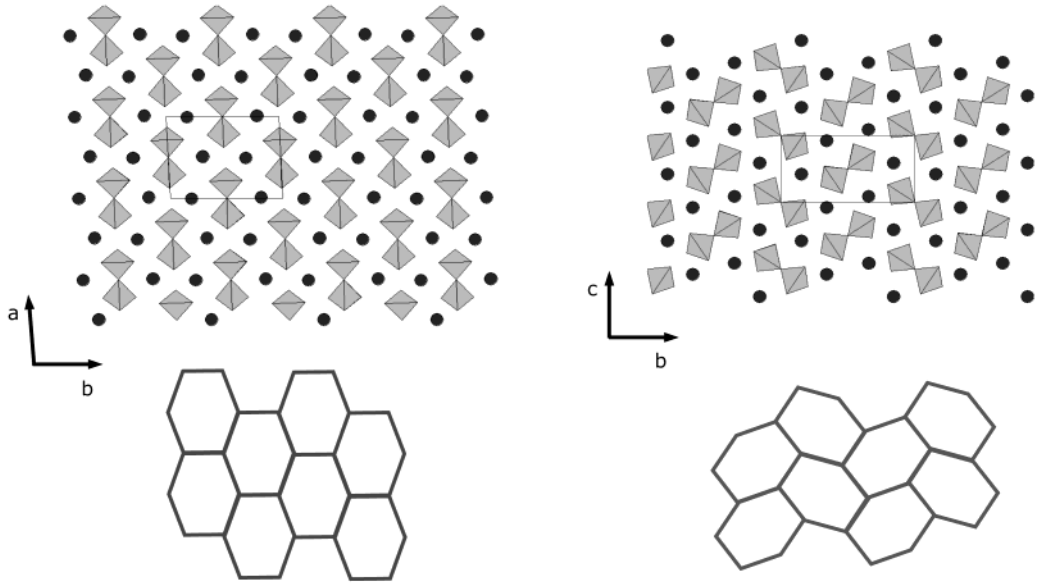

a) β-$Fe_2P_2O_7$ b) γ-$Fe_2P_2O_7$

Figure 3. Comparison between the two polymorphic forms of $Fe_2P_2O_7$. The figure shows the diphosphate groups distributions on top and the schematic picture of the Fe hexagonal arrangements on the bottom.

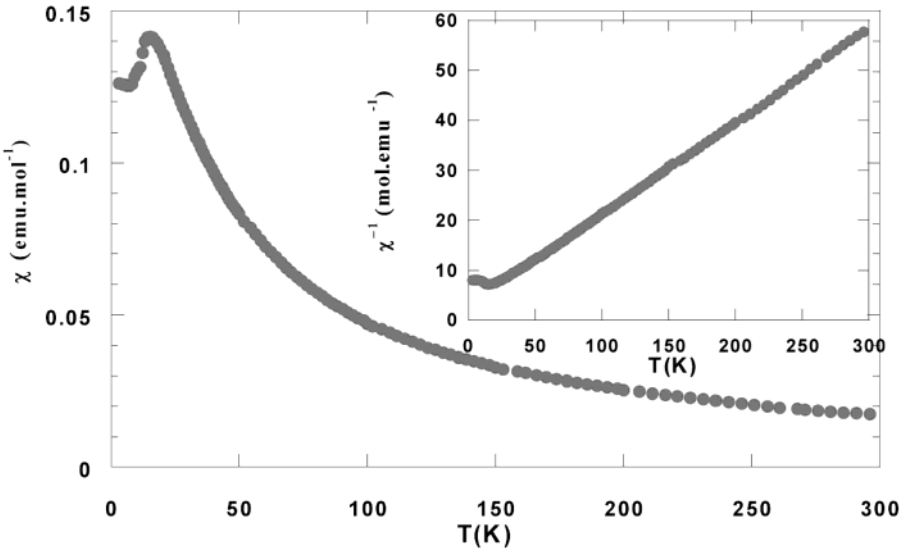

Figure 4. Magnetic susceptibility, χ, and inverse magnetic susceptibility, χ^{-1}, plotted as a function of temperature for $Fe_2P_2O_7$.

Table 4. Cell Parameters for $M_2P_2O_7$ (M = Divalent First Series Transition Metal)

$M_2P_2O_7$	l.p.[a]	i.p.[a]	s.p.[a]	β (deg)	S.G.	V[a]	ref
			α-Polymorph				
$Co_2P_2O_7$	13.248(6)	9.004(3)	8.345(3)	104.6(1)	$B2_1/c$	963.3	19
$Ni_2P_2O_7$	13.093	8.974	8.275	104.94	$B2_1/c$		20
$Cu_2P_2O_7$	9.164(3)	8.113(3)	6.895(2)	109.62(2)	$C2/c$	428.9	21
$Zn_2P_2O_7$	20.068(15)	9.099(8)	8.259(6)	106.35(5)	$I2/c$	1447.1	22
			β-Polymorph				
$Mn_2P_2O_7$	8.584(1)	6.633(1)	4.546(1)	102.67(1)	$C2/m$	252.6(1)	23
$Fe_2P_2O_7$	8.484(2)	6.649(2)	4.488(1)	103.89(3)[b]	$C\bar{1}$	245.4	11, 12
$Co_2P_2O_7$	8.526(4)	6.640(3)	4.524(2)	102.59(3)	$A2/m$	250.0(2)	24
$Ni_2P_2O_7$	8.239	6.501	4.480	101.14	$C2/m$		25
$Cu_2P_2O_7$	8.118(10)	6.827(8)	4.576(6)	108.85(10)	$C2/m$	240.0	26
$Zn_2P_2O_7$	8.29(1)	6.61(1)	4.51(1)	105.4(2)	$C2/m$	238.3	27
			γ-Polymorph				
$Fe_2P_2O_7$	9.896(1)	5.2077(7)	4.4668(6)	97.516(2)	$P2_1/c$	228.22(5)	
$Co_2P_2O_7$ [c]	9.923(1)	5.339(1)	4.488(1)	97.45(2)	$P2_1/a$	235.72(6)	28
$Ni_2P_2O_7$	9.913(5)	5.212(3)	4.475(3)	97.46(10)	$P2_1/a$	229.3	29
$Zn_2P_2O_7$	16.482(3)	13.335(2)	4.9504(5)	α,β,γ = 90	$Pbcm$	1088.1(2)	30

[a] l.p. = longest parameter; i.p. = intermediate parameter; s.p. = shortest parameter (Å). V = cell volume (Å^3). [b] α = 90.04°, γ = 92.82(3)°. [c] There is a fourth $Co_2P_2O_7$ polymorph with space group $P2_1/c$ and cell parameters a = 7.008(4) Å, b = 8.345(3) Å, c = 9.004(3) Å, β = 113.84(6)°.

of the susceptibility. As can be observed in the Figure 4 inset, the susceptibility data can be fitted to the Curie−Weiss law over a wide temperature range, that is, 20−300 K, $\chi = C/(T - \theta)$, $C = N_A(\mu_{eff})^2/3k$, where C is the Curie constant, θ the Weiss constant, N_A Avogadro's number, μ_{eff} the effective magnetic moment, and k Boltzmann's constant.

The fitting of the linear part of the $\chi^{-1}-T$ plot yields a value of the magnetic moment of 4.73 μ_B, which agrees with that theoretically expected for Fe^{2+} in a high-spin state.[18] The Weiss constant θ was found to be −21 K, which is indicative of the existence of antiferromagnetic ordering in the Fe^{2+} sublattice. This behavior is fully confirmed with the onset of a net maximum in the χ vs T curve at 12.5 K; this maximum can be ascribed to the Neel temperature.

The analysis, in detail, of the structure (Figures 1 and 2) shows that there are two main different pathways to explain these antiferromagnetic interactions. The first one involves a superexchange mechanism of the type Fe−O−Fe that takes place between the FeO_6 octahedra sharing edges in the *bc* plane of the structure with three octahedra, which are the nearest neighbors. As result of this, a zigzag superexchange Fe−O−Fe pathway along the *c*- or *b*-axis is operative. However, along the *a*-axis the FeO_6 octahedra are connected by P_2O_7, units giving rise to a super-superexchange mechanism ac-

(18) Boudreaux, E. A.; Mulay, L. N. *Theory of Molecular Paramagnetism*; A Wiley-Interscience Publication; John Wiley & Sons: New York, 1976.
(19) Krishnamachari, N.; Calvo, C. *Acta Crystallogr.* **1972**, *B28*, 2883.
(20) Lukaszewicz, K. *Bull. Acad. Polon. Sci., Ser. Sci. Chim.* **1967**, *15*, 47.
(21) Effenberger, H. *Acta Crystallogr.* **1990**, *C46*, 691.
(22) Robertson, B. E.; Calvo, C. *J. Solid State Chem.* **1970**, *1*, 120.
(23) Stefanidis, T.; Nord, A. G. *Acta Crystallogr.* **1984**, *C40*, 1995.
(24) El Belghitti, A.; Boukhari, A. *Acta Crystallogr.* **1994**, *C50*, 482.
(25) Pietraszko, A.; Lukaszewicz, K. *Bull. Acad. Polon. Sci., Ser. Sci. Chim.* **1968**, *16*, 183.
(26) Robertson, B. E.; Calvo, C. *Mater. Res. Bull.* **1993**, 1241.
(27) Calvo, C. *Can. J. Chem.* **1965**, *43*, 1147.
(28) Kobashi, D.; Kohara, S.; Yamakawa, J.; Kawahara, A. *Acta Crystallogr.* **1977**, *C53*, 1523.
(29) Masse, R.; Guitel, J. C.; Durif, A. *Mater. Res. Bull.* **1979**, *14*, 337.
(30) Bataille, T.; Bernard-Rocherulle, P.; Louer, D. *J. Solid State Chem.* **1998**, *140*, 62.

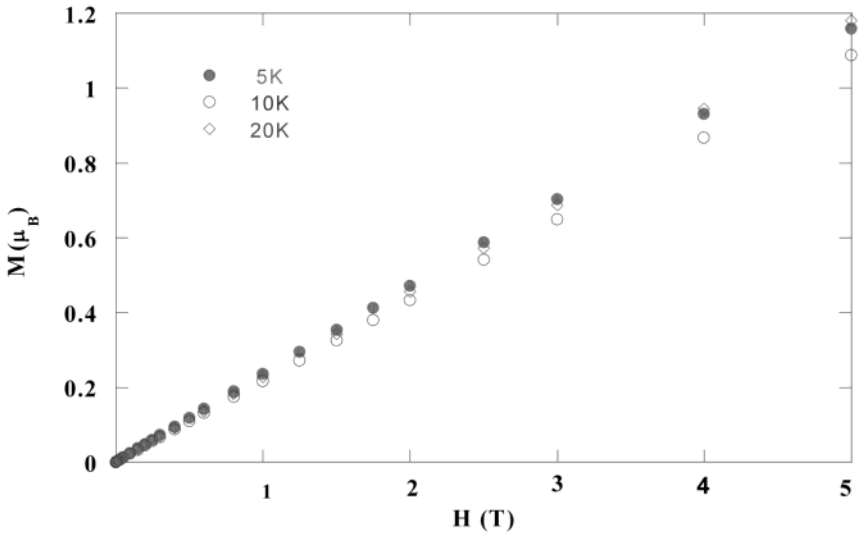

Figure 5. M vs H isotherms obtained below the Neel temperature.

cording to the sequence of atoms involved in the pathway of the type Fe−O−P−O−Fe. The relatively large distance, 4.47 Å, between the iron atoms and angles very far from 180° (angles involved: Fe−O−P = 121.84°, O−P−O = 105.71°, P−O−Fe = 140.59°) lead to a very poor d-orbital overlap, which is consistent with the low values of 12.5 K estimated for the Neel temperature associated with this compound.

Magnetization isotherms obtained below the Neel temperature, Figure 5, follow a linear variation in the whole range of the magnetic field strength characteristic of the mentioned antiferromagnetic order and metamagnetic (field induced) transitions have not been observed up to 5 T. We are currently performing neutron diffraction experiments to obtain a deeper knowledge of the low-temperature magnetic behavior and to determine the magnetic structure of this phosphate.

Acknowledgment. This work was supported by the Spanish DGICYT under Project No. MAT2001-1433.

Supporting Information Available: X-ray crystallographic data (CIF). This material is available free of charge via the Internet at http://pubs.acs.org.

CM034137A